Article

Cell Reports

Contribution of RNA Degradation to Intrinsic and Extrinsic Noise in Gene Expression

Graphical Abstract

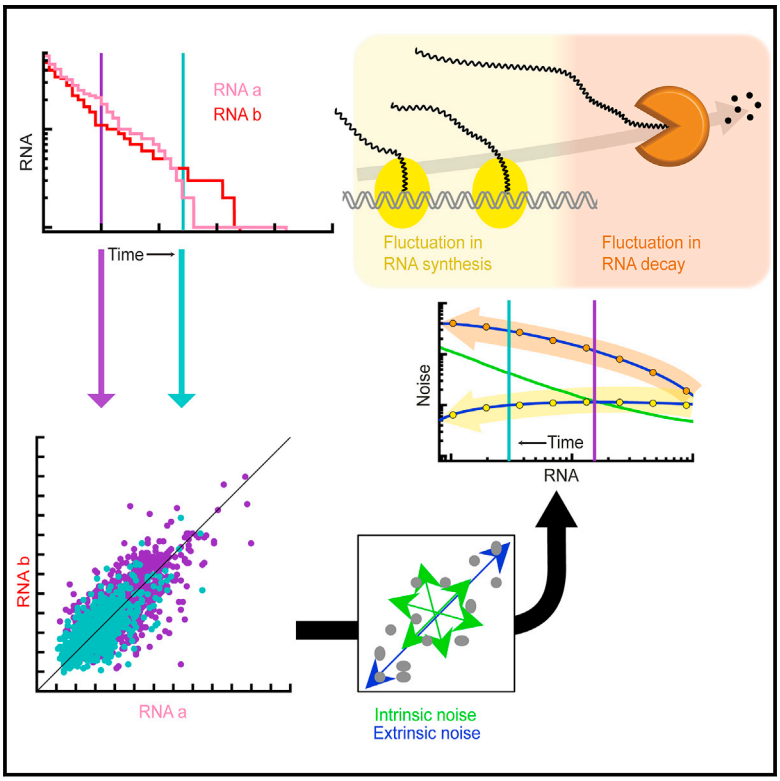

Authors

Antoine Baudrimont, Vincent Jaquet, Sandrine Wallerich, Sylvia Voegeli, Attila Becskei

Correspondence

attila.becskei@unibas.ch

In Brief

Baudrimont et al. show that fluctuations in transcription and RNA degradation can be distinguished by assessing whether extrinsic noise increases during decay. Unstable RNAs are more susceptible to noise, but the activity of the enzymes that degrade them fluctuates less in comparison to those that target stable mRNAs.

Highlights

- We assessed how RNA degradation affects cell-to-cell variability in RNA expression
- Extrinsic noise increases during RNA decay when RNA degradation fluctuates
- Unstable mRNAs are more susceptible to noise than stable mRNAs
- The activity of Xrn1, which targets unstable mRNAs, has small fluctuations

Baudrimont et al., 2019, Cell Reports *26*, 3752–3761
March 26, 2019
https://doi.org/10.1016/j.celrep.2019.03.001

CellPress

OPEN ACCESS
CellPress

Cell Reports
Article

Contribution of RNA Degradation to Intrinsic and Extrinsic Noise in Gene Expression

Antoine Baudrimont,[1,2,3] Vincent Jaquet,[1,2] Sandrine Wallerich,[1] Sylvia Voegeli,[1] and Attila Becskei[1,4,*]
[1]Biozentrum, University of Basel, Klingelbergstrasse 50/70, 4056 Basel, Switzerland
[2]These authors contributed equally
[3]Present address: Max F. Perutz Laboratories, University of Vienna, Vienna, Austria
[4]Lead Contact
*Correspondence: attila.becskei@unibas.ch
https://doi.org/10.1016/j.celrep.2019.03.001

SUMMARY

Genetically identical cells contain variable numbers of molecules, even if the cells share the same environment. This stochastic variability is prominent when molecules have low abundance, which is the case for mRNA noise. Most studies focused on how transcription affects mRNA noise, and little is known about the role of RNA degradation. To discriminate the fluctuations in these processes during the decay of a pair of reporter mRNAs, we quantified the uncorrelated intrinsic and the correlated extrinsic noise using single-molecule RNA FISH. Intrinsic noise converges to the Poisson level during the decay. mRNAs that have a short half-life are more susceptible to extrinsic noise than stable mRNAs. However, the Xrn1 exonuclease and the NMD pathways, which degrade mRNAs rapidly, were found to have lower fluctuation, which mitigates the noise of the short-lived mRNAs. This permits low variability across the entire range of mRNA half-lives.

INTRODUCTION

Single-cell studies have revealed a substantial cell-to-cell variability in the expression of genes (Gasch et al., 2017; Newman et al., 2006; Symmons and Raj, 2016). This variability, noise in gene expression, can significantly alter the behavior of regulatory networks, causing deviations from the familiar deterministic dynamics (Hsu et al., 2016a, 2016b; Shahrezaei et al., 2008).

A main cause of the stochastic variability is the low number of molecules in a cell, which is typically the case for nucleic acid polymers, exemplified by genes and mRNA molecules. There are one to four copies of each gene in a cell, depending on the cellular ploidy and replication state. Similarly, most mRNA molecules are present at less than 10 copies in unicellular organisms, such as yeast or bacteria (Arbel-Goren et al., 2016; Wadsworth et al., 2017; Zenklusen et al., 2008). Since both components of transcription, genes and mRNAs, have low numbers in a cell, transcription is a noisy process. Noise in the expression of one gene can also propagate to another gene through biochemical control. Thus, noise has multiple sources and can be decomposed in different ways (Mitchell and Hoffmann, 2018). A dual-reporter method has been developed to distinguish two sources of noise, the intrinsic and extrinsic noise (Elowitz et al., 2002). The random collision of molecules that triggers the biochemical reactions introduces substantial fluctuations when the copy number of the molecule is low; these fluctuations are not shared by the two alleles of the gene due to their distinct spatial localization and thus are uncorrelated (Shahrezaei et al., 2008). At the same time, fluctuations in the molecular pathways controlling the expression of both alleles of a gene generate correlated fluctuations (Hilfinger and Paulsson, 2011). Generally, the uncorrelated and correlated fluctuations correspond to the intrinsic and extrinsic noise measured with the dual-reporter method (Shahrezaei et al., 2008). The determination of the origins of the extrinsic noise has been a main goal of single-cell systems biology (Shahrezaei and Swain, 2008).

Most studies have focused on how stochasticity is affected by transcription, including the control by promoters, replication, elongation, and chromatin dynamics (Huber et al., 2016; Peterson et al., 2015; Tripathi and Chowdhury, 2008; Yang et al., 2014). In addition to the above processes that affect the rate of RNA synthesis, RNA degradation is the second determinant of RNA abundance. However, it is less clear how mRNA degradation affects noise.

All mRNAs in the budding yeast are transcribed by the RNA polymerase II, whereas two different, evolutionarily conserved, enzymes can degrade them. The Xrn1 exonuclease degrades them in the 5′-to-3′ direction, while the exosome proceeds in the opposite, 3′-to-5′ direction. Recent evidence suggests that mRNA turnover in yeast is very rapid, with a median half-life of around 2 min (Baudrimont et al., 2017; Wada and Becskei, 2017). Most mRNAs with short half-lives are degraded by the Xrn1 exonuclease. Stable mRNAs, as well as all mRNAs in the absence of Xrn1, are degraded by the exosome. While all mRNAs are subject to physiological turnover, mutated or defective mRNAs are recognized by surveillance pathways, which can steer even stable mRNAs to rapid degradation. The nonsense-mediated decay (NMD) is a classical surveillance pathway, which targets mRNAs with premature stop codons (PMS). PMS frequently occurs in unspliced mRNAs that leak from the nucleus into the cytoplasm or can also arise due to transcriptional infidelity (Bonde et al., 2014; He and Jacobson, 2015). mRNAs recognized by NMD are degraded also by the Xrn1 (He et al., 2003).

In this work, we show with the help of stochastic modeling that the major sources of noise in mRNA expression, transcription

and degradation, can be distinguished by measuring noise in mRNA expressed from a dual-reporter system upon shutting off their expression. The dual-reporter method has been mainly used with fluorescent proteins (Raser and O'Shea, 2004) and rarely with mRNAs encoding the fluorescent proteins (Raj et al., 2006). Here, we adapted the two-reporter method to measure the endogenous mRNAs with single-molecule fluorescence in situ hybridization (FISH).

RESULTS

Fluctuations in RNA Synthesis and Decay Generate Similar Distributions of Steady-State RNA Expression

We simulated simple models of gene expression to assess how RNA degradation affects noise. Here, we quantified noise, η_{tot}, in terms of the coefficient of variation (CV), $\eta_{tot} = CV\langle RNA\rangle = sd\langle RNA\rangle/\langle RNA\rangle$; $sd\langle RNA\rangle$ and $\langle RNA\rangle$ denote the SD and the mean of the distribution of RNA numbers in a cell population, respectively. In this work, we use the term noise for the steady-state variability in the RNA abundances. We reserve the term fluctuation to denote the variations in the activity of transcription and degradation, which we estimate by modeling.

If an RNA species is synthesized constantly and degraded by a first-order process, the copy number adopts a Poisson distribution (Thattai, 2016). We decomposed noise into intrinsic and extrinsic components, as defined in Equation 1. The squared total noise is the sum of the squared intrinsic and extrinsic noise: $\eta^2_{tot} = \eta^2_{\text{int}} + \eta^2_{ext}$ (Swain et al., 2002). When the stochastic expression of the two alleles is independent (Figures 1A and 1B, birth-death model), the number of the two RNA reporters displays a round scatter, and thus noise is purely intrinsic (Figure 1B).

In the more complex two-state promoter model, RNA is synthesized only when the promoter is activated. The active state is established through the random molecular encounter of the promoter and the activator (Peccoud and Ycart, 1995). The activation is reversible: the promoter becomes inactive when the activator dissociates from it. In this two-state promoter model, the noise is stronger but the stochastic gene expression of the two alleles remains independent (Figure 1B, with no shared fluctuations), meaning that all noise is intrinsic. Next, we extended the two-state promoter model to include the natural fluctuations in the activity of the enzymes that synthesize and degrade the RNA. These natural fluctuations can arise due to the stochastic synthesis, decay, or biochemical control of enzymes. The intrinsic noise did not change considerably but the scatter became elongated reflecting the appearance of the extrinsic noise, which arises due to the correlated fluctuations in RNA synthesis or degradation since each of these processes affects both RNA reporters (Figure 1B). The intrinsic and extrinsic noise is similar independently of whether the fluctuations are introduced through RNA synthesis or degradation (Figures 1B and S1). This similarity makes it difficult to determine the origin of RNA extrinsic noise from steady-state measurements.

Increase in Extrinsic Noise over the Course of RNA Decay Is a Hallmark of Fluctuations in RNA Degradation

Therefore, we examined how noise varies during RNA decay upon shutting off gene expression (Figures 1C–1E, S2, and S3; Table S1). In the birth-death model, the intrinsic noise increases throughout the time course of the decay as the number of RNA molecules declines. There is an inverse relation between them, $\eta^2_{\text{int}} = 1/\langle RNA\rangle$, which is characteristic of the Poisson distribution. With the two-state promoter model, intrinsic noise is initially super-Poisson, which reflects the fact that multiple mRNAs are transcribed while the promoter is active; in other words, the burst size is larger than 1. This initially super-Poisson intrinsic noise converges to a Poisson noise level, as the decay goes on (Figure 1C). A similar convergence can be seen when the RNA synthesis or degradation rate fluctuates (Figures 1D and 1E). Thus, intrinsic noise behaves relatively uniformly across the models.

On the other hand, the extrinsic noise displays a marked difference with respect to the origin of fluctuations. When the RNA synthesis rate fluctuates, the extrinsic noise remains approximately constant over the course of the decay (Figure 1D). Conversely, extrinsic noise increases when the concentration of the RNA-degrading enzyme fluctuates (Figure 1E). The differential effect of these fluctuations can be understood intuitively. The fluctuations in transcription do not play a role after shutting off gene expression, and thus mRNAs inherit the cell-to-cell variability they experience in steady state. Thus, extrinsic noise due to transcription remains constant during decay. On the other hand, the cell-to-cell variability of the RNA abundance can be further amplified during the course of the decay when the degradation rate fluctuates. This effect is particularly strong, when the fluctuations in RNA degradation are slow and the RNA half-life is short (Figure S2). Thus, we argued that fluctuations in transcription and degradation can be distinguished by measuring the extrinsic noise with the dual-reporter assay over the time course of the RNA decay.

The Adoption of the Dual-Reporter Method to RNA Molecules Permits the Measurement of Intrinsic and Extrinsic Noise in RNA Expression

The dual-reporter method was developed to measure noise using fluorescent proteins. Its adoption to endogenous mRNAs requires an appropriate design and detection. In order to be distinguishable with single-molecule FISH (smFISH), the two RNA reporters must contain sufficiently long heterologous sequences. At the same time, they have to be kinetically similar. In order to meet these two opposing requirements, we have relied on a strategy that we developed to preserve the dynamic range of RNA expression when parts of the gene sequence are replaced (Hsu et al., 2016b). We have inserted a GFP or mCherry sequence into the middle part of a gene of interest and placed each allele under the control of the *GAL1* promoter (Figure 2A; Tables S2 and S3). Their expression did not cause growth defect. Each reporter construct was transformed into a haploid strain, which were then mated to obtain the dual-reporter diploid strains. Each allele was integrated into identical chromosomal loci. The heterologous sequences permitted the clear distinction of the two mRNA reporters by smFISH (Figure 2B).

Most of the mRNAs in yeast have short half-lives (<5 min) and few have long ones (>5 min) (Baudrimont et al., 2017). We have selected the unstable *TSL1* and stable *PGK1* mRNAs to construct the respective reporter genes. Next, we measured their half-lives: cells were induced by galactose, which activates

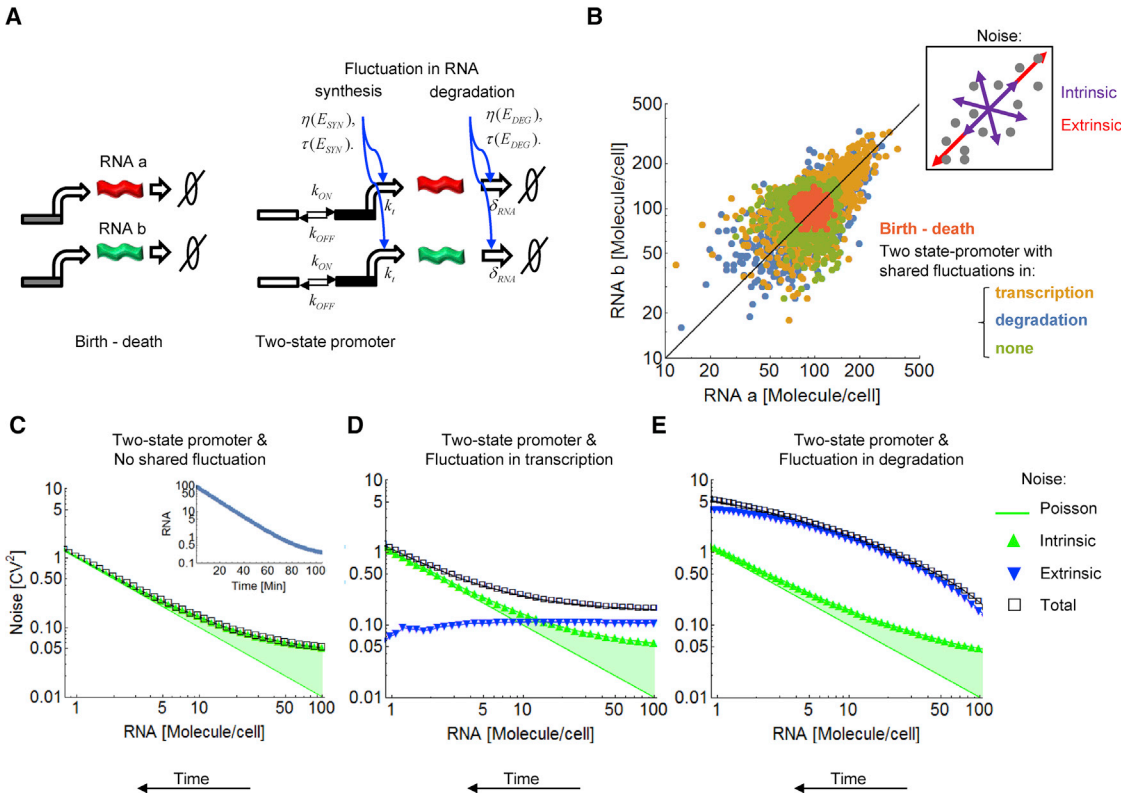

Figure 1. Fluctuations in RNA Synthesis and Degradation Each Have Their Characteristic Effects on Extrinsic Noise during Simulated RNA Decay

(A) Models of expression of kinetically equivalent mRNAs. The simplest model (birth-death, left panel) includes RNA synthesis and degradation. This model was extended with the following reactions (two-state promoter, right panel): transitions between active and inactive states of the promoter, and birth and death of enzymes that synthesize and degrade RNAs. These enzymes introduce fluctuations that affect both RNA reporters. The reaction parameters are indicated for the extended model. k_{ON} and k_{OFF} are the promoter activation and inactivation rate constants, respectively. k_t and δ_{RNA} are the RNA synthesis (transcription) and RNA degradation rate constants, respectively. $\eta(E_{SYN})$and $\eta(E_{DEG})$ denote the fluctuation intensities in RNA synthesis and degradation, respectively. $\tau(E_{SYN})$ and $\tau(E_{DEG})$ denote the lifetimes of the respective fluctuations (see also Quantification and Statistical Analysis).

(B) Distribution of molecule numbers of mRNA alleles. The following noise values were obtained in steady state with the indicated models: birth-death (η^2_{int} = 0.01, η^2_{ext} = 0; red), two-state promoter (η^2_{int} = 0.05, η^2_{ext} = 0; green), two-state promoter with fluctuations in transcription (η^2_{int} = 0.057, η^2_{ext} = 0.106; yellow), and two-state promoter with fluctuations in degradation (η^2_{int} = 0.047, η^2_{ext} = 0.137; blue). The half-life of the mRNA is 10 min. Transcription rate constant (k_t) was set so that RNA = 100 molecules in the deterministic model. Further parameter values are described in Table S1. The inset illustrates the copy number scatter characteristic of the intrinsic and extrinsic noise.

(C–E) Intrinsic and extrinsic noise as a function of the RNA molecule numbers over the course of RNA decay. The decay is started by setting k_t to a basal value, which is 500 times less than the initial value. The same model parameters were used as in (B). The difference between the measured intrinsic noise and Poisson noise is denoted by green shading. In the two-state promoter model with no shared control, all noise is intrinsic (C). The shared control in transcription (D) or degradation (E) generates extrinsic noise, which is approximately constant or increasing, respectively, over the course of the decay.

the *GAL1* promoter through the Gal4 activator (Figure 2C). Upon the rapid replacement of the galactose-containing medium with a galactose-free medium, gene expression was shut off. We then quantified RNA by qPCR (Table S4). The estimated half-lives of the two mRNA reporters were essentially identical, and similar to that of the respective parent mRNA. Thus, this strategy permits the adoption of the dual-reporter assay to RNAs.

The Combination of Noise Time Series with the Histogram Dataset Improves the Parameter Estimation

First, we studied the stable *PGK1* mRNA. The steady-state noise of the two *PGK1* RNA reporters was similar (CV = 0.349 and CV = 0.318). Furthermore, the molecule numbers of the two reporters displayed strongly overlapping distributions (Figure 3A), an important experimental criterion for the quantification of the intrinsic and extrinsic noise.

To estimate the fluctuations in transcription and degradation and the parameters in the two-state promoter model, we progressively constrained the range of parameter values to improve the fit to the observations. This was done in three stages: we used analytical formulas in the first stage, and stochastic simulations in the second and third stages (Table S5; Quantification and Statistical Analysis).

In the first stage, we took advantage of an analytical expression, which links parameters of the two-state promoter model (with no shared fluctuations) to noise (see Equation 10). Since

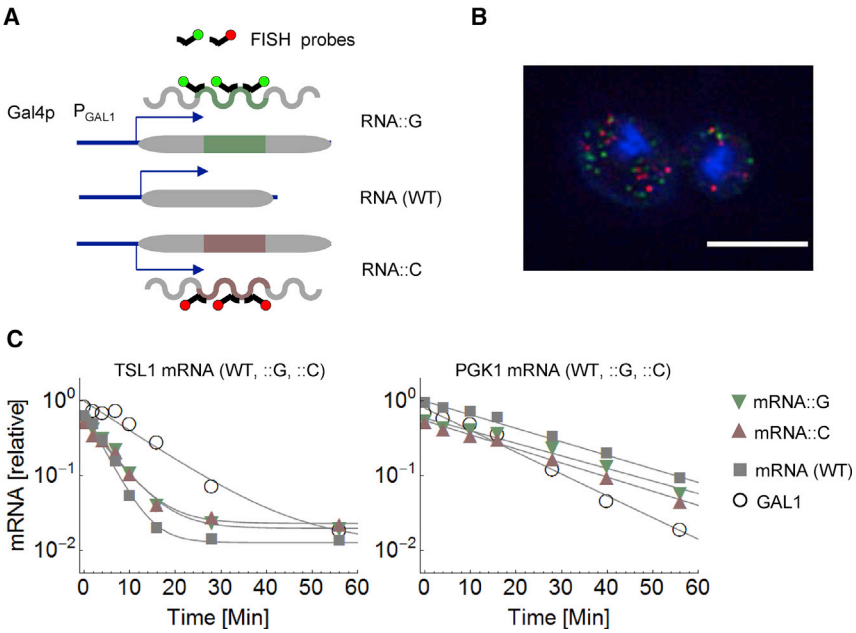

Figure 2. The Decay of the RNA Expressed from the Two Alleles of the Dual-Reporter System

(A) The two reporter alleles were obtained by the insertion (::G and ::C) of heterologous sequences (GFP and mCherry). The probes hybridizing to these sequences were used to detect the RNA molecules.

(B) Fluorescence microscopy images of cells expressing the *TSL1*::G and *TSL1*::C mRNAs. The cells were imaged 10 min after shutting off gene expression induced by 0.5% galactose. Scale bar: 5 μm.

(C) The decay of the mRNAs with and without the inserted heterologous sequences (GFP or Cherry), upon shutting off expression driven by the *GAL1* promoter. The following half-lives ($t_{1/2}$) were fitted for the mRNAs quantified by qPCR: *TSL1*::G (3.6 min), *TSL1*::C (3.6 min), and *TSL1* (2.5 min); *PGK1*::G (17.9 min), *PGK1*::C (16.3 min), and *PGK1* (16.6 min) mRNAs.

this model does not contain extrinsic source of fluctuations, the measured intrinsic noise was substituted into this equation. Three parameter values were also substituted into the equation. The decay rate was fitted with the exponential function, and the mean copy number of the RNA was measured. A third parameter, the fractional saturation of the *GAL1* promoter, was constrained based on an earlier study (Gencoglu et al., 2017). The fractional saturation reflects the percentage of promoters bound by the transcription factor Gal4 averaged over a cell population or a time period. Upon these substitutions, we constrained the domain of parameter values in the two-state promoter model and transferred it to the second stage.

In the second stage, we extended the two-state promoter model with fluctuations in RNA synthesis and degradation. We simulated this model stochastically with a matrix of parameter values and assessed how the solutions fit the observed steady-state histograms and the extrinsic noise as it varies over the decay time series. When we calculated fits separately to each of these datasets, the parameter values that generated good fits occupied different but overlapping domains in the parameter space (blue and yellow in Figure 3B). When we performed the fitting with the combined dataset, the fluctuation intensity was restricted to a narrower domain of values (red in Figure 3B), implying that the power of the fitting is better when performed with both observations. In contrast to the intensity, the lifetime of the fluctuations was spread all over the parameter space (Figure S4A). The best-fit values for the promoter saturation were high, larger than 0.9 (Figure S4C).

The Stochastic Deviant Effect Slows Down the RNA Decay but Only Minimally

In the third stage, we sampled parameter values randomly from this narrower domain defined with the joint fit and fitted the stochastic model to the RNA decay profiles, as well. This is important because the decay can deviate from an exponential function when the fluctuations in the degradation are strong, especially when the RNA half-life is short (Figure S3). By letting the half-life vary around the value fitted with the exponential function, we fitted the half-life based on the stochastic model, which generates the decay profile as the mean RNA changes over the course of the decay. Upon obtaining the best fit, we used the same value to plot the exponential function (yellow thick line in Figure 3D) and the mean RNA obtained with the stochastic model (black line in Figure 3D). Despite the identical parameters, a small but increasing deviation can be observed between the deterministic and stochastic decay profiles with the progress of the time because the fluctuations slow down the decay.

As the *PGK1* RNA number declines, noise increases (Figure 3C). The initially super-Poisson intrinsic noise converged to the Poisson level ($\eta^2_{int} = 1/\langle RNA \rangle$), confirming expectations based on the two-state promoter models. Furthermore, the extrinsic noise increased markedly over the course of the decay, which is a hallmark of the fluctuations in RNA degradation. In the late stage of the decay, the extrinsic noise declined because the mean RNA number converges to the basal expression (Figure S2). The best-fit parameters reveal strong fluctuations both in RNA synthesis and degradation.

NMD Is Subject to Small Fluctuations

Next, we studied how fluctuations change when the RNA is degraded rapidly. Short-lived mRNAs have higher intrinsic and extrinsic noise (Figure S1). Thus, they are inherently more susceptible to fluctuations. In order to assess this effect with a minimal change in the reporter construct, we inserted a PMS into the open-reading frame, which will steer the *PGK1* mRNA to the NMD pathway (Figure 4A). Indeed, the PMS reduced the mRNA half-life around five times.

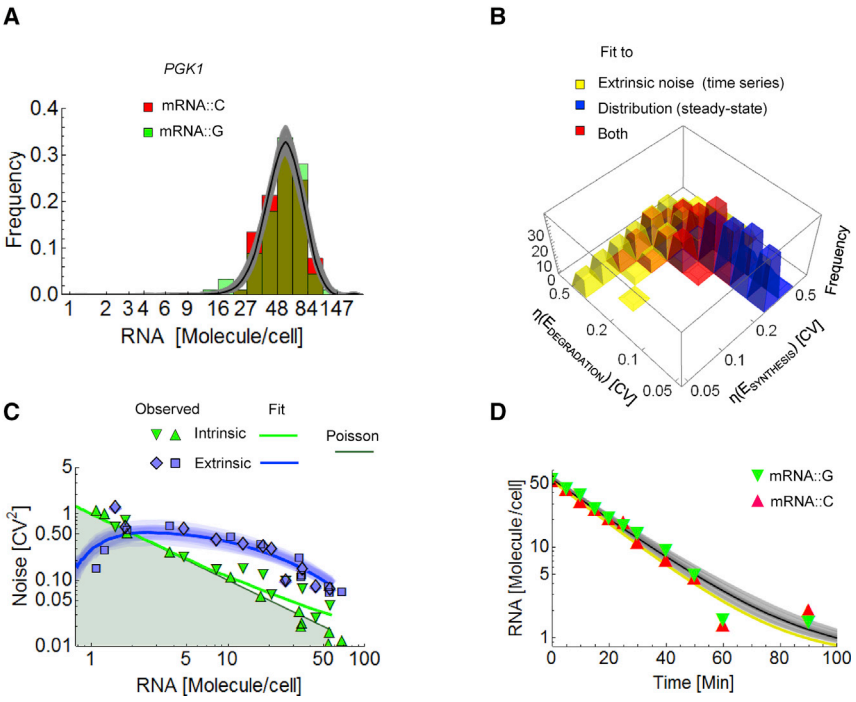

Figure 3. Intrinsic and Extrinsic Noise in the Expression of the *PGK1* mRNA over the Course of the Decay

The thick black or blue lines denote the best fit (parameter values in Table S6). The gray or blue bands denote the model solutions with the 30 best parameter fits.

(A) Steady-state distribution of the *PGK1* mRNAs expressed from the two insertional alleles. The two distributions are identical. (The null hypothesis that the datasets have the same distributions is not rejected at the 5% level based on the Kolmogorov-Smirnov test; p = 0.81.)

(B) The histogram shows the distribution of the 200 best fits for the fluctuation intensities. The goodness of model fits (*RSSE*) was calculated separately for the steady-state distribution (blue) and the extrinsic noise time series (yellow), and for their combination (red).

(C) The intrinsic (triangles) and extrinsic (quadrilaterals) noise measured in two biological replicates (first replicate: downward triangle and diamond; second replicate: upward triangle and square). The Poisson noise, $\eta^2_{int} = 1/\langle RNA \rangle$, is indicated by a dark green line.

(D) Mean of the distribution of RNA reporter molecules expressed from each allele, during the decay. The thick yellow line is the solution of the deterministic exponential function (Equation 2) with the same parameters as the respective stochastic model (black line).

The intrinsic noise of *PGK1-PMS* was similar to that of its parent RNA, *PGK1*. We plotted the noise expected from the change in the RNA half-life due to the PMS. This change, including a compensation of the transcription rate to reflect the new mean RNA, is expected to increase extrinsic noise around four times. Surprisingly, the measured extrinsic noise was substantially lower than the expected one (Figure 4B). Indeed, the fitted fluctuations in the degradation were lower in the *PGK1-PMS* mRNA (Figure S4B), which implies that the surveillance pathway operates at a lower noise level than the pathway targeting the stable wild-type (WT) *PGK1* mRNA.

Fluctuation Intensities in RNA Degradation Estimated Based on the Dual-Reporter System Are Corroborated by the Observations with the Semi-shutoff System

Next, we wanted to see whether the promoter de-induction method we employed to study the decay interferes with the measurement. Therefore, we compared the existing dual-reporter method to an alternative system to shut off gene expression (Figures 5A and 5B). In these cells, the expression of one of the RNA reporters is constant, and thus remains in stationary state, while the expression of the second one is shut off. Therefore, these cells were dubbed the "semi-shutoff" system (Figures 5A and 5C). To build this strain, we retained the original reporters but placed them under the control of different promoters. One of them was driven by the TET-OFF system, in which the transcriptional activator tTA binds to the *tet* operators in the promoter. Gene expression was shut down by adding doxycycline, which dissociates tTA from the promoter. The reporter with the constant expression was controlled by GEV, a synthetic transcriptional activator whose activity can be tuned with estradiol (for more details, see Experimental Model and Subject Details). The two reporters were driven by promoters of very similar sequences, in which only the transcription factor binding sites differed. The GEV recognizes the original Gal4 binding sites in the *GAL1* promoter. In the modified *GAL1* promoter, the Gal4 binding sites were replaced with *tet* operators to be recognized by tTA. The activator domains of the transcription factors GEV and tTA are also identical in this system. With this system, we analyzed *TSL1*, a representative of the mRNAs with rapid turnover. By adjusting the estradiol concentration, we obtained similar steady-state expression levels of the two RNA reporters (Figure 5C, at 0 min). The half-life we measured was similar to that obtained using the GAL system (Figures 5C and S5C).

As a substitute for extrinsic noise, we calculated the correlation coefficient from the single-cell abundances of the two RNA reporters (see Quantification and Statistical Analysis). The correlation declined gradually from around 0.6 to one-half of this value around 10 min after the shutoff (Figure 5D). The fitted fluctuation intensities in the RNA degradation obtained with the dual-reporter and the semi-shutoff system were similar (Figures 5D and 5E), confirming the low-intensity fluctuations in the degradation of *TSL1* mRNA.

Degradation by the Xrn1 Exonuclease Is Subject to Low-Intensity Fluctuations, Which Mitigates the High Noise Susceptibility of Short-Lived mRNAs

Our results so far indicate that fluctuations are stronger in the degradation of the stable *PGK1* mRNA in comparison to the unstable *PGK1-PMS* and *TSL1* mRNAs (Figure S6A). In the case of

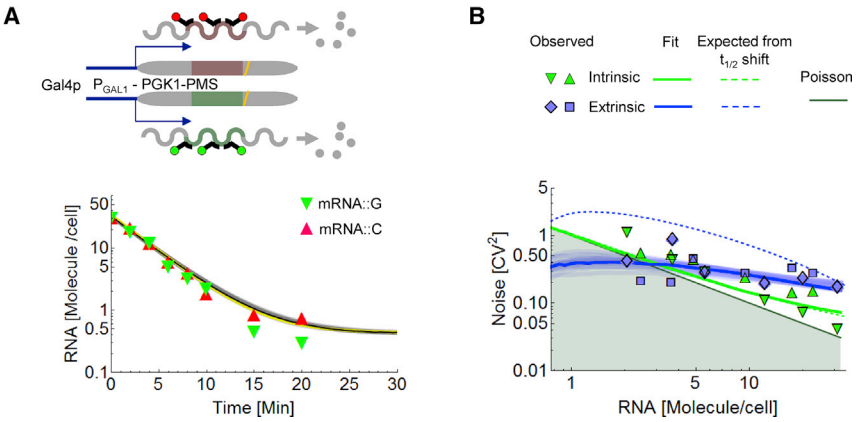

Figure 4. Changes in Noise Due to the Introduction of the *PMS* into the *PGK1*

The blue line denotes the best fit (parameter values in Table S6). The gray or blue bands denote the model solutions with the 30 best parameter fits. Symbols and fits used as in Figure 3.

(A) Scheme of the dual-reporter system expressing the *PGK1-PMS* (top panel). The PMS (yellow stripe in the scheme) is positioned 225 triplets downstream of the start codon in the context of the *PGK1* sequence. The thick yellow line in the plot is the solution of the deterministic exponential function with the same parameters as in the stochastic model.

(B) The intrinsic and extrinsic noise measured in two biological replicates. The dashed blue and green lines represent the extrinsic and intrinsic noise expected from changing solely the RNA half-life among the *PGK1* parameters, owing to the PMS. With the exception of the compensatory transcription rate k_t = 9.71 min^{-1}, all parameters are the same as for *PGK1*.

the *TSL1* and *PGK1–PMS*, the estimated fluctuation lifetimes were scattered broadly in the parameter space (Figure S6B); only in the case of the *PGK1* did it occupy a narrower range. Next, we examined whether the estimated intensities of the fluctuations depend on the lifetimes. Therefore, we restricted the parameter domain of the lifetimes to around 10 min and plotted the corresponding fluctuation intensities. The fluctuations in the RNA degradation of *PGK1* were significantly higher than for *PGK1-PMS* (Figure S6C), which confirms our prior conclusions.

Both NMD targets and naturally short-lived mRNAs are degraded predominantly by the 5′→3′ exonuclease Xrn1 (Figure 6A) (Baudrimont et al., 2017). Thus, we argued that Xrn1 may account for the low fluctuation in the degradation of these mRNAs. Therefore, we deleted *XRN1* and examined *TSL1* decay in this cell background (Figure S7A). The decay was, as expected, substantially slower (Figure S5). The intrinsic noise was similar to the other examined mRNAs: it converged to the Poisson level, which suggests that the deletion does not introduce uncorrelated fluctuations (Figure 6D). However, the extrinsic noise was considerably higher than expected from the change in the half-life. This confirms our hypothesis that Xrn1 activity is affected by small fluctuations, which mitigates the noise of short-lived mRNAs (Figures 6B and S7B).

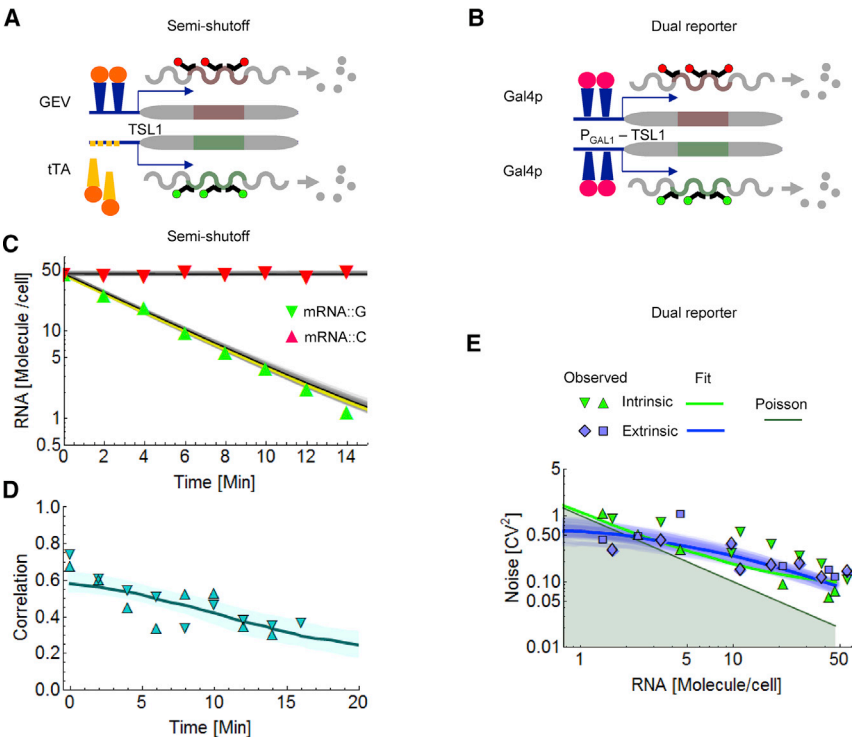

Figure 5. Estimation of Fluctuations in *TSL1* RNA Degradation by Shutting Off the Expression of One or Two mRNA Reporters

(A and B) In the dual-reporter strain (B and E), the expression of both reporters is shut off since Gal4 controls both *GAL1* promoters. In the semi-shutoff strain (A, C, and D), the level of only one of the reporters declines upon dissociation of tTA from the promoter.

(C) The decay of the mRNA upon shutting off the expression of the $P_{[tetO]4inGAL1}$ – *TSL1*::G. The estimated RNA half-life is 2.7 min.

(D) Correlation between the decaying *TSL1*::G and the stationary *TSL1*::C. Further details as in Figure 3. The parameter estimation was performed as with the dual-reporter system, but the Pearson correlation coefficient was used instead of the extrinsic noise.

(E) The intrinsic and extrinsic noise measured in the dual-reporter system (two biological replicates: triangles and quadrilaterals).

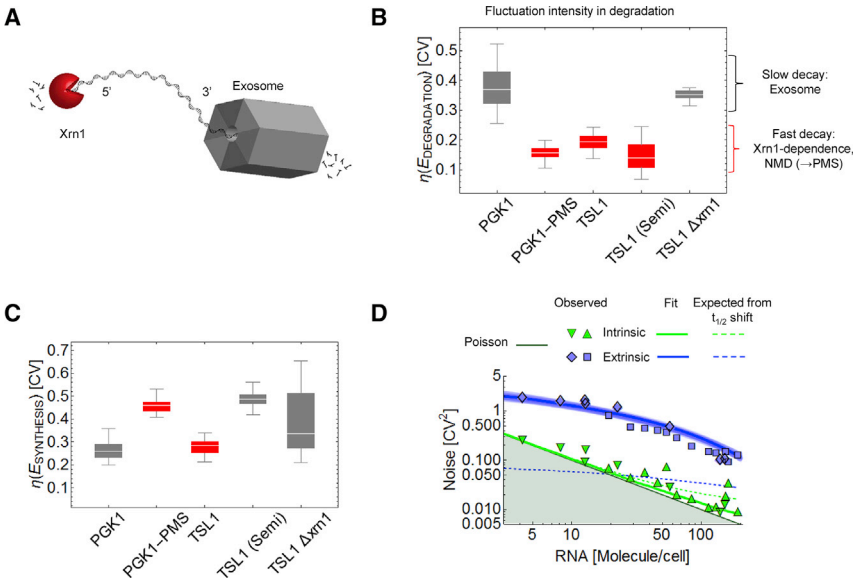

Figure 6. Relative Contribution of Fluctuations in mRNA Synthesis and Degradation to Noise in RNA Expression

(A) The scheme of the RNA degradation pathways. Xrn1 degrades unstable mRNAs in 5′-to-3′ direction, while the exosome degrades all mRNAs in 3′-to-5′ direction. The larger size of the exosome indicates that it is a multi-subunit complex.

(B and C) The 30 best fits for the intensities of the fluctuations in the RNA degradation (B) and synthesis (C) (*CV*, whisker-boxplots with 25th to 75th percentiles). The following mean values (with 95% confidence intervals) of the $\eta(E_{DEGRADATION})$ were obtained: 0.37 (0.34, 0.40) for *PGK1*, 0.16 (0.15, 0.17) for *PGK1*-PMS, 0.20 (0.18, 0.21) for *TSL1*, 0.15 (0.13, 0.18) for *TSL1* (semi-shutoff), and 0.35 (0.34, 0.36) for *TSL1* (Δxrn1) mRNAs. The estimates for the $\eta(E_{SYNTHESIS})$: 0.26 (0.24, 0.28) for *PGK1*, 0.46 (0.45, 0.47) for *PGK1*-PMS, 0.28 (0.26, 0.29) for *TSL1*, 0.49 (0.47, 0.50) for *TSL1* (semi-shutoff), and 0.38 (0.33, 0.43) for *TSL1* (Δ*xrn1*) mRNAs.

(D) The intrinsic and extrinsic noise measured (two biological replicates: triangles and quadrilaterals) in the *TSL1* dual-reporter system in Δ*xrn*1 cells. The blue line denotes the best fit (parameter values in Table S6). The dashed blue and green lines represent the extrinsic and intrinsic noise expected from changing solely the RNA half-life among the *TSL1* parameters, owing to the deletion of *XRN1*. With the exception of the compensatory transcription rate $k_t = 3.20\ \text{min}^{-1}$, all parameters are the same as for *TSL1* in WT cells (Figure 3).

DISCUSSION

Unstable mRNAs are more susceptible to noise than stable ones. Our results suggest that cells counter this susceptibility by low-noise degradation pathways. This has important theoretical and practical implications.

Fluctuations in degradation rate can cause a deviation from the classical exponential decay profiles (Figure S3) and can interfere with the discrimination of noise sources when using the dual-reporter system (Shahrezaei et al., 2008). Extrinsic noise reflects normally the fluctuations shared by the two alleles. However, a theoretical analysis revealed that shared fluctuations could leak into the intrinsic noise, especially, when the activity or amount of the enzyme that degrades the RNA or proteins strongly fluctuates (Shahrezaei et al., 2008). In this case, a stochastic deviant effect makes the mean value of a variable in the stochastic model differ from the value of the same variable in the deterministic model. This effect can be observed both in steady state (Figure S1) and during decay (Figure S3). A strong deviant effect can arise in models in which two components, such as RNA and a RNA-degrading enzyme, interact multiplicatively, and the activity of both of them fluctuate or alternate between two states. (Deneke et al., 2013; Kuwahara and Schwartz, 2012; McShane et al., 2016). It is important to note that the decay profile can deviate from an exponential function due to causes other than the deviant kinetics.

The observed decay profile deviated from the expected deterministic exponential only minimally in our measurements. Similarly, the intrinsic noise approached the Poisson level over the course of RNA decay in all our constructs, which implies stochastic deviant effect is small. Thus, the intrinsic noise measured with the dual-RNA reporter construct is not disturbed by the leakage of shared fluctuations.

In a genome-wide study of fluorescent protein fusions, low- and high-noise proteins were found to have a CV of around 0.1 and 0.3, respectively (Newman et al., 2006). The enzyme involved in the degradation of short-lived mRNAs, Xrn1, has a particularly low noise (CV = 0.13–0.15 in cells grown in synthetic and rich media), which is in good agreement with our estimates. The exosome is a multi-subunit complex (Kowalinski et al., 2016). Interestingly, the components of the exosome, which targets the more stable mRNAs, have higher noise levels (CV = 0.15–0.19) (Newman et al., 2006), which is in a qualitative agreement with our findings. We estimated even stronger fluctuations in the pathway targeting stable RNAs (CV = 0.3–0.4). Some of the differential noise level is likely to be copy-number dependent: Xrn1 is present at around 700–1,000 copies per cell, while the above exosome components are present only at 150–200 copies per cell (Newman et al., 2006). It is important to note that we estimated activity fluctuations and not merely concentration fluctuations, and the activity is influenced by multiple factors, such as localization, binding interactions, and covalent modifications. The multimerization of the stochastically expressed subunits of the exosome may further amplify noise in the enzymatic activity.

The fluctuations in RNA synthesis were strong in our gene constructs (Figure 6C), which is not surprising since the strong *GAL1* promoter that drives the transcription has been known to be relatively noisy (Blake et al., 2006). Interestingly, the fluctuations in synthesis are stronger in *PGK1-PMS* than in *PGK1* despite the similarity of the two genes. The *PGK1-PMS* has a considerably shorter half-life and it reacts more sensitively to fast fluctuations. Live imaging of fluorescent proteins revealed that the fluctuations are best described by a range of fluctuation lifetimes as

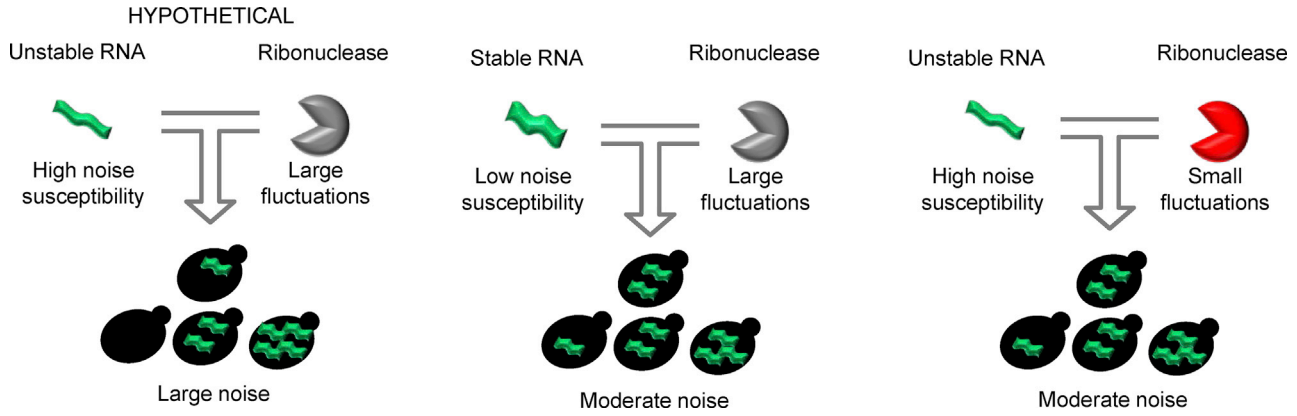

Figure 7. Scheme of Stochastic Regulatory Combinations in RNA Degradation

Stable (long-lived) mRNAs are inherently less susceptible to noise, while unstable (short-lived) mRNAs are more susceptible to noise. Consequently, when a short-lived mRNA is degraded by enzymes with large fluctuations (gray Pac-Man symbol), noise in RNA expression is large. We have not observed this combination (hypothetical case). Unstable mRNAs are degraded by enzymes with small fluctuations, which mitigates noise (right panel). Stable mRNAs are degraded by enzymes with large fluctuations but the inherently low noise susceptibility of stable mRNAs yields moderate noise in RNA expression.

characterized by a power spectrum (Austin et al., 2006). Thus, it is plausible that fast components of the fluctuations in RNA synthesis are strong in the *GAL1/PGK1* hybrid promoter but only *PGK1-PMS* reacts to them in a detectable way since they are averaged out by the more stable *PGK1.* For the *TSL1* mRNA in Δ*xrn1* cells, the estimated lifetime and the intensity of the transcriptional fluctuations were even linked, as evidenced by a negative correlation between them (Figure S6D).

The model we use for the parameter estimation is concise and supported by multiple observations. However, future studies will be required to refine the model and parameters. Without aiming at a comprehensive list, we mention four aspects below. First, we obtained well-constrained estimates for the intensities of the fluctuations in RNA degradation, but the estimated lifetimes were scattered more broadly. Thus, live imaging will be required in future studies to estimate the lifetime of the fluctuations. Second, we assume that the RNA degradation rate is linearly proportional to the concentration of the ribonucleases. Saturation of these enzymes or the interaction between the enzymes and the genes or mRNAs encoding the enzymes (Sun et al., 2012) may cause deviations from linearity, but this is unlikely to influence the relative values of the estimated fluctuation intensities. Third, the value we use for the promoter saturation was estimated in our earlier study employing protein mass spectrometry (Gencoglu et al., 2017). This helped to restrict the range of the promoter deactivation rates. It is important to note that the promoter deactivation rate and the RNA synthesis rate are strongly coupled, and it is difficult to determine their independent absolute values (To and Maheshri, 2010). This coupling is particularly evident at low transcription rates: even when the promoter is active, transcription occurs randomly, with the possibility of having long intervals without mRNAs being synthesized. Fourth, the RNA half-lives we obtain with gene control are shorter than those obtained in most prior studies, including those using transcriptional inhibition and metabolic labeling (Carneiro et al., 2019). However, our gene control method is consistent because the half-lives estimated upon shutting off gene expression with synthetic promoters are similar to the values obtained when the expression of the endogenous genes was shut off (Baudrimont et al., 2017; Wada and Becskei, 2017).

In summary, we show that the fluctuations in the RNA degradation pathway are moderate enough not to cause major stochastic deviations but strong enough to cause substantial cell-to-cell variability upon shutting off gene expression. These findings have important physiological implications. The fluctuations in RNA degradation are particularly relevant for those genes whose transcription undergoes rapid temporal changes. For example, many genes are transcribed only for a short period of time during the cell cycle whereupon the expressed RNA decays. A large cell-to-cell variability in this period would interfere with the precision required to orchestrate the events in the cell division cycle (Barik et al., 2016). The low fluctuations in the Xrn1 activity are of benefit not only to the regular RNA targets but also to mRNAs with nonsense codons (NMD). Thus, the surveillance pathway does not only reduce genetic noise, in terms of aberrant messages, but also the gene expression noise due to the small fluctuations in the pathway.

We have found two regulatory combinations in this work (Figure 7): unstable mRNAs subject to small fluctuations and stable mRNAs subject to strong fluctuations in the RNA degradation pathways. We did not detect a combination where strongly fluctuating pathways degrade unstable mRNAs. Therefore, we expect that a pronounced deviant effect is unlikely to be common. In this way, noise in RNA expression is low in the whole range of RNA half-lives observed in the genome.

STAR★METHODS

Detailed methods are provided in the online version of this paper and include the following:

- KEY RESOURCES TABLE
- CONTACT FOR REAGENT AND RESOURCE SHARING

SUPPLEMENTAL INFORMATION

Supplemental Information can be found online at https://doi.org/10.1016/j.celrep.2019.03.001.

ACKNOWLEDGMENTS

We thank Takeo Wada for the help with the strain constructions and Mukund Thattai for reading the manuscript. This work was supported by grants from SystemsX.ch (StoNets).

AUTHOR CONTRIBUTIONS

A. Becskei designed the experiments. A. Baudrimont, S.W., and S.V. performed the experiments. V.J. performed the simulations and data analysis. A. Becskei wrote the paper.

DECLARATION OF INTERESTS

The authors declare no competing interests.

Received: May 9, 2018
Revised: November 26, 2018
Accepted: February 27, 2019
Published: March 26, 2019

REFERENCES

Aguilera, L.U., Zimmer, C., and Kummer, U. (2017). A new efficient approach to fit stochastic models on the basis of high-throughput experimental data using a model of IRF7 gene expression as case study. BMC Syst. Biol. *11*, 26.

Arbel-Goren, R., Tal, A., Parasar, B., Dym, A., Costantino, N., Muñoz-García, J., Court, D.L., and Stavans, J. (2016). Transcript degradation and noise of small RNA-controlled genes in a switch activated network in *Escherichia coli*. Nucleic Acids Res. *44*, 6707–6720.

Austin, D.W., Allen, M.S., McCollum, J.M., Dar, R.D., Wilgus, J.R., Sayler, G.S., Samatova, N.F., Cox, C.D., and Simpson, M.L. (2006). Gene network shaping of inherent noise spectra. Nature *439*, 608–611.

Barik, D., Ball, D.A., Peccoud, J., and Tyson, J.J. (2016). A stochastic model of the yeast cell cycle reveals roles for feedback regulation in limiting cellular variability. PLoS Comput. Biol. *12*, e1005230.

Baudrimont, A., Voegeli, S., Viloria, E.C., Stritt, F., Lenon, M., Wada, T., Jaquet, V., and Becskei, A. (2017). Multiplexed gene control reveals rapid mRNA turnover. Sci. Adv. *3*, e1700006.

Blake, W.J., Balázsi, G., Kohanski, M.A., Isaacs, F.J., Murphy, K.F., Kuang, Y., Cantor, C.R., Walt, D.R., and Collins, J.J. (2006). Phenotypic consequences of promoter-mediated transcriptional noise. Mol. Cell *24*, 853–865.

Bonde, M.M., Voegeli, S., Baudrimont, A., Séraphin, B., and Becskei, A. (2014). Quantification of pre-mRNA escape rate and synergy in splicing. Nucleic Acids Res. *42*, 12847–12860.

Carneiro, R.L., Requião, R.D., Rossetto, S., Domitrovic, T., and Palhano, F.L. (2019). Codon stabilization coefficient as a metric to gain insights into mRNA stability and codon bias and their relationships with translation. Nucleic Acids Res. Published online January 30, 2019. https://doi.org/10.1093/nar/gkz033.

Deneke, C., Lipowsky, R., and Valleriani, A. (2013). Complex degradation processes lead to non-exponential decay patterns and age-dependent decay rates of messenger RNA. PLoS ONE *8*, e55442.

Elowitz, M.B., Levine, A.J., Siggia, E.D., and Swain, P.S. (2002). Stochastic gene expression in a single cell. Science *297*, 1183–1186.

Gasch, A.P., Yu, F.B., Hose, J., Escalante, L.E., Place, M., Bacher, R., Kanbar, J., Ciobanu, D., Sandor, L., Grigoriev, I.V., et al. (2017). Single-cell RNA sequencing reveals intrinsic and extrinsic regulatory heterogeneity in yeast responding to stress. PLoS Biol. *15*, e2004050.

Gencoglu, M., Schmidt, A., and Becskei, A. (2017). Measurement of in vivo protein binding affinities in a signaling network with mass spectrometry. ACS Synth. Biol. *6*, 1305–1314.

Haddad, F., Qin, A.X., Giger, J.M., Guo, H., and Baldwin, K.M. (2007). Potential pitfalls in the accuracy of analysis of natural sense-antisense RNA pairs by reverse transcription-PCR. BMC Biotechnol. *7*, 21.

He, F., and Jacobson, A. (2015). Nonsense-mediated mRNA decay: degradation of defective transcripts is only part of the story. Annu. Rev. Genet. *49*, 339–366.

He, F., Li, X., Spatrick, P., Casillo, R., Dong, S., and Jacobson, A. (2003). Genome-wide analysis of mRNAs regulated by the nonsense-mediated and 5′ to 3′ mRNA decay pathways in yeast. Mol. Cell *12*, 1439–1452.

Hilfinger, A., and Paulsson, J. (2011). Separating intrinsic from extrinsic fluctuations in dynamic biological systems. Proc. Natl. Acad. Sci. USA *108*, 12167–12172.

Hsu, C., Jaquet, V., Gencoglu, M., and Becskei, A. (2016a). Protein dimerization generates bistability in positive feedback loops. Cell Rep. *16*, 1204–1210.

Hsu, C., Jaquet, V., Maleki, F., and Becskei, A. (2016b). Contribution of bistability and noise to cell fate transitions determined by feedback opening. J. Mol. Biol. *428*, 4115–4128.

Huber, F., Bunina, D., Gupta, I., Khmelinskii, A., Meurer, M., Theer, P., Steinmetz, L.M., and Knop, M. (2016). Protein abundance control by non-coding antisense transcription. Cell Rep. *15*, 2625–2636.

Kowalinski, E., Kögel, A., Ebert, J., Reichelt, P., Stegmann, E., Habermann, B., and Conti, E. (2016). Structure of a cytoplasmic 11-subunit RNA exosome complex. Mol. Cell *63*, 125–134.

Kuwahara, H., and Schwartz, R. (2012). Stochastic steady state gain in a gene expression process with mRNA degradation control. J. R. Soc. Interface *9*, 1589–1598.

McShane, E., Sin, C., Zauber, H., Wells, J.N., Donnelly, N., Wang, X., Hou, J., Chen, W., Storchova, Z., Marsh, J.A., et al. (2016). Kinetic analysis of protein stability reveals age-dependent degradation. Cell *167*, 803–815.e21.

Mitchell, S., and Hoffmann, A. (2018). Identifying noise sources governing cell-to-cell variability. Curr. Opin. Syst. Biol. *8*, 39–45.

Moison, C., Arimondo, P.B., and Guieysse-Peugeot, A.L. (2011). Commercial reverse transcriptase as source of false-positive strand-specific RNA detection in human cells. Biochimie *93*, 1731–1737.

Mueller, F., Senecal, A., Tantale, K., Marie-Nelly, H., Ly, N., Collin, O., Basyuk, E., Bertrand, E., Darzacq, X., and Zimmer, C. (2013). FISH-quant: automatic counting of transcripts in 3D FISH images. Nat. Methods *10*, 277–278.

Newman, J.R., Ghaemmaghami, S., Ihmels, J., Breslow, D.K., Noble, M., DeRisi, J.L., and Weissman, J.S. (2006). Single-cell proteomic analysis of *S. cerevisiae* reveals the architecture of biological noise. Nature *441*, 840–846.

Paulsson, J. (2004). Summing up the noise in gene networks. Nature *427*, 415–418.

Peccoud, J., and Ycart, B. (1995). Markovian modeling of gene-product synthesis. Theor. Popul. Biol. *48*, 222–234.

Peterson, J.R., Cole, J.A., Fei, J., Ha, T., and Luthey-Schulten, Z.A. (2015). Effects of DNA replication on mRNA noise. Proc. Natl. Acad. Sci. USA *112*, 15886–15891.

Raj, A., Peskin, C.S., Tranchina, D., Vargas, D.Y., and Tyagi, S. (2006). Stochastic mRNA synthesis in mammalian cells. PLoS Biol. *4*, e309.

Raser, J.M., and O'Shea, E.K. (2004). Control of stochasticity in eukaryotic gene expression. Science *304*, 1811–1814.

Sanft, K.R., Wu, S., Roh, M., Fu, J., Lim, R.K., and Petzold, L.R. (2011). StochKit2: software for discrete stochastic simulation of biochemical systems with events. Bioinformatics *27*, 2457–2458.

Schindelin, J., Arganda-Carreras, I., Frise, E., Kaynig, V., Longair, M., Pietzsch, T., Preibisch, S., Rueden, C., Saalfeld, S., Schmid, B., et al. (2012). Fiji: an open-source platform for biological-image analysis. Nat. Methods *9*, 676–682.

Shahrezaei, V., and Swain, P.S. (2008). The stochastic nature of biochemical networks. Curr. Opin. Biotechnol. *19*, 369–374.

Shahrezaei, V., Ollivier, J.F., and Swain, P.S. (2008). Colored extrinsic fluctuations and stochastic gene expression. Mol. Syst. Biol. *4*, 196.

Sun, M., Schwalb, B., Schulz, D., Pirkl, N., Etzold, S., Larivière, L., Maier, K.C., Seizl, M., Tresch, A., and Cramer, P. (2012). Comparative dynamic transcriptome analysis (cDTA) reveals mutual feedback between mRNA synthesis and degradation. Genome Res. *22*, 1350–1359.

Swain, P.S., Elowitz, M.B., and Siggia, E.D. (2002). Intrinsic and extrinsic contributions to stochasticity in gene expression. Proc. Natl. Acad. Sci. USA *99*, 12795–12800.

Symmons, O., and Raj, A. (2016). What's luck got to do with it: single cells, multiple fates, and biological nondeterminism. Mol. Cell *62*, 788–802.

Thattai, M. (2016). Universal Poisson statistics of mRNAs with complex decay pathways. Biophys. J. *110*, 301–305.

Thattai, M., and van Oudenaarden, A. (2001). Intrinsic noise in gene regulatory networks. Proc. Natl. Acad. Sci. USA *98*, 8614–8619.

To, T.L., and Maheshri, N. (2010). Noise can induce bimodality in positive transcriptional feedback loops without bistability. Science *327*, 1142–1145.

Tripathi, T., and Chowdhury, D. (2008). Transcriptional bursts: a unified model of machines and mechanisms. Europhys. Lett. *84*, 6.

Wada, T., and Becskei, A. (2017). Impact of methods on the measurement of mRNA turnover. Int. J. Mol. Sci. *18*, 2723.

Wadsworth, G.M., Parikh, R.Y., Choy, J.S., and Kim, H.D. (2017). mRNA detection in budding yeast with single fluorophores. Nucleic Acids Res. *45*, e141.

Yang, S., Kim, S., Rim Lim, Y., Kim, C., An, H.J., Kim, J.H., Sung, J., and Lee, N.K. (2014). Contribution of RNA polymerase concentration variation to protein expression noise. Nat. Commun. *5*, 4761.

Zenklusen, D., Larson, D.R., and Singer, R.H. (2008). Single-RNA counting reveals alternative modes of gene expression in yeast. Nat. Struct. Mol. Biol. *15*, 1263–1271.

STAR★METHODS

KEY RESOURCES TABLE

REAGENT or RESOURCE	SOURCE	IDENTIFIER
Chemicals, Peptides, and Recombinant Proteins		
Doxycycline hyclate	Formedium	CAT# DOX25
β- Estradiol	Sigma-Aldrich	CAT# E8875-250MG
Formaldehyde solution	Sigma-Aldrich	CAT# F8775
Poly-L-lysine	Sigma-Aldrich	CAT# P4707
D(+) – raffinose pentahydrate	Formedium	CAT# RAF04
Critical Commercial Assays		
ProLong Gold medium	Thermo Fisher Scientific	CAT# P36930
Deposited Data		
RNA expression measured by single molecule RNA FISH (mean value, intrinsic and extrinsic noise).	This paper; Mendeley Data	https://data.mendeley.com/datasets/jpd7jmsj95/draft?a=3819df83-93a8-48ea-8721-167196bf2999
Experimental Models: Organisms/Strains		
S. cerevisiae strains (see Table S3)	This paper	N/A
Oligonucleotides		
Primers for qPCR (see Table S4)	This paper	N/A
Probe sequence for smFISH (see Table S7)	This paper	N/A
Recombinant DNA		
Plasmid integrated in *S. cerevisiae* (see Table S2)	This paper	N/A
Software and Algorithms		
Stellaris RNA FISH Probe Designer	LGC Biosearch Technologies	https://www.biosearchtech.com/support/tools/design-software/stellaris-probe-designer
FISH-Quant	Mueller et al., 2013	V2d http://bitbucket.org/muellerflorian/fish_quant/src
MATLAB	MathWorks	RRID:SCR_001622
WOLFRAM MATHEMATICA	Wolfram Research	RRID:SCR_014448
SoftWorx 4.1.2	GE Healthcare (previously Applied Precision)	http://incelldownload.gehealthcare.com/bin/download_data/SoftWoRx/7.0.0/SoftWoRx.htm
StochKit	Sanft et al., 2011	https://github.com/StochSS/StochKit
Fiji	Schindelin et al., 2012	RRID:SCR_002285

CONTACT FOR REAGENT AND RESOURCE SHARING

Further information and requests for resources and reagents should be directed to and will be fulfilled by the Lead Contact, Attila Becskei (attila.becskei@unibas.ch).

EXPERIMENTAL MODEL AND SUBJECT DETAILS

Construction of plasmids and strains

The plasmids expressing the WT and insertional RNAs (Table S2) were integrated into the chromosome of the BY4741 and BY4742 strains (Table S3). These strains are derivatives of the yeast *Saccharomyces cerevisiae* S288C. Upon transformation of the cells, we selected reporter constructs having a single-copy integration at the FIG1 locus. By mating the two haploid cells, each containing one reporter, we obtained diploid cells.

To construct the plasmids, a GFP (denoted as::G) or a mCherry (denoted as::C) sequence was inserted into the mid-part of the *TSL1*, *PGK1* or *PGK1-PMS* open-reading frames (ORF). In the *PGK1-PMS*, the *PGK1* ORF was mutated at position 225 codons (i.e., 675 bp) downstream of the start codon to create a PMS. The GFP and mCherry were used solely as hybridization sequences for the single molecule FISH (smFISH). The promoter P_{GAL1} controlled the RNA expression in the dual-reporter strains. In the *GAL1* promoter, we replaced the 87 bp sequence upstream of the start codon by a 130 bp *PGK1* or a 60 bp *TSL1* sequence upstream of the

start codons in order to include the respective 5′UTR sequences. To include the 3′UTR sequences, 239 and 200 bp sequences downstream of the *PGK1* and *TSL1* coding sequences were cloned.

In the semi-shutoff strain, the RNA reporter was expressed under the control of P_{GAL1} or $P_{[tetO]4inGAL1}$. These related promoters were regulated by the transcription activators GEV and tTA, respectively. The original GAL1 promoter was controlled by GEV (Gal4-DBD – ER – VP16), which is a fusion protein of a Gal4 DNA-binding domain, an estradiol receptor (ER) and a VP16 activation domain (Hsu et al., 2016b). The second promoter, $P_{[tetO]4inGAL1}$, was obtained by replacing the four Gal4p binding sites in the *GAL1* promoter by tet operators. The resulting $P_{[tetO]4inGAL1}$ was controlled by tTA, which is a fusion protein consisting of the TetR DNA-binding protein and the VP16 activation domain. Thus, the expression of the two RNA reporters was driven by similar promoter sequences and was controlled by the same transcriptional activation domain (VP16). The $P_{[tetO]4inGAL1}$ was placed upstream of the *TSL1::G* ORF. The *TSL1::C* construct is identical to that in the dual-reporter assay. The strains expressed constitutively the tTA and GEV activators.

Growth conditions and shut-off experiments

When the cells are grown in synthetic complete (SC, 2% raffinose, 0.005% glucose) medium containing 0.5% galactose, the Gal4p activates the expression of reporter genes under the control of the GAL promoter. The overnight culture was refreshed and let to grow for 4 hours to reach an OD600 of around 0.5. At this mid-log phase, the decay was initiated by filtering the culture through a cellulose acetate membrane. The cells were resuspended in the same medium without galactose. The amount of the *GAL1* mRNA started to decline exponentially after a time lag. The half-lives of the mRNAs were determined using the time points after this lag.

The semi shut-off cells were grown in SC media with 60 nM estradiol to maintain the constitutive expression of *TSL1::C*. The expression of the *TSL1::G* RNA was shut off by adding doxycycline at a final concentration of 10 μg/ml to dissociate tTA from the promoter.

METHOD DETAILS

RNA extraction, reverse transcription and qPCR

The collection of the sample, RNA extraction, reverse transcription and qPCR were performed as previously described (Baudrimont et al., 2017), with the following modification: oligo(dT) was used to prime reverse transcription. The sequences of the qPCR primers are shown in Table S4.

Single molecule mRNA FISH

Collection of samples, cell preparation and quantification of mRNA were performed as described (Baudrimont et al., 2017), with a modification to allow the detection of two different fluorescent probe sets. Briefly, cells were fixed in 3.7% formaldehyde and transferred to coverslips coated with poly-L-lysine. After the hybridization of the probes and washing of the samples, cells were mounted in Prolong® Gold medium and cured overnight at room temperature before imaging.

The Quasar 670 (LGC, Biosearch technologies, US) probes, which recognize the mCherry sequence were imaged with the CY5 channel and the Quasar 570 probes, which recognize the GFP sequence, were imaged with the TRITC channel. meGFP and mCherry probes are labeled at their 3′ ends with Quasar® 570 and 670 (Stellaris probes), respectively. Each sequence was covered with 34 probes (Table S7). The probes were designed with the Stellaris RNA FISH Probe Designer. The cells were imaged with an Olympus Plan Apo N (60x, Numerical Aperture: 1.42) objective, with an auxiliary magnification of 1.6x. The DAPI, FITC, TRITC and CY5 filters were used with 100% ND, bin 1, exposure time of 0.8 (32%), 1, 0.8, 1 s respectively. SoftWorx 4.1.2 was used for the deconvolution of the images. The auto-fluorescence of the cells (FITC) was used to define the cell boundaries in cells that contained a nucleus as visualized with the DAPI filter, which was performed with Fiji (Schindelin et al., 2012). The RNA molecules were identified with FISH-Quant, a MATLAB toolbox (Mueller et al., 2013).

QUANTIFICATION AND STATISTICAL ANALYSIS

Measurement of noise

The intrinsic and extrinsic noise was calculated according to the dual-reporter method (Elowitz et al., 2002), in both the simulations and experimental measurements:

$$\eta^2_{\text{int}} = \frac{\left\langle (a-b)^2 \right\rangle}{2\langle a\rangle \cdot \langle b\rangle}; \quad \eta^2_{ext} = \frac{\langle ab\rangle - \langle a\rangle \cdot \langle b\rangle}{\langle a\rangle \cdot \langle b\rangle}; \tag{1}$$

Analysis of time series and determination of mRNA half-lives

To estimate mRNA half-life, we used the exponential function (Equation 2) for the measurements with the qPCR and for the first stage of the fitting with the stochastic model with smFISH data (see below).

$$RNA(t) = RNA_b + RNA(0)e^{-\delta_{RNA}t} \tag{2}$$

$RNA(0)$and RNA_b denote the initial and basal expression, respectively. The fitting was performed with Mathematica. The fitted RNA_b can differ when measured with qPCR and smFISH because qPCR can detect antisense RNA in addition to sense RNA. Furthermore, the qPCR measurements can be affected by concentration dependent self-priming during the reverse transcription (Haddad et al., 2007; Moison et al., 2011), which is not the case for smFISH.

Stochastic models

To assess how fluctuations in RNA synthesis and degradation affect stochastic gene expression, we have constructed simple stochastic models of gene expression. Each model describes the expression of RNA variants from the two gene alleles ($i = 1, 2$). In the two simplest models ((3) and (6)), the birth-death and the two-state promoter models, there are no reactions shared by both alleles. In the extended models, the fluctuations introduced through the shared process of RNA synthesis and degradation affect both alleles, which leads to the appearance of extrinsic noise, in the sense of the dual reporter method.

The models include variables and parameters (rate constants). The variables denote the following components: *RNA* (RNA), *I* (promoter in the inactive state), *A* (promoter in the active state), E_{SYN} (Enzyme that synthesizes the RNA) and E_{DEG} (Enzyme that degrades the RNA). The subscript *i* denotes the allele. The parameters denote the following rate constants: k_t (RNA synthesis), δ_{RNA} (RNA decay), k_{ON} (promoter activation), k_{OFF} (promoter inactivation), k_E (enzyme synthesis) and δ_E (enzyme degradation).

Birth-death model

Each RNA allele (RNA_i) is synthesized constitutively and is degraded by a first order process.

$$\emptyset \xrightarrow{k_t} RNA_i$$

$$RNA_i \xrightarrow{\delta_{RNA}} \emptyset \tag{3}$$

This birth-death model results in a Poisson distribution:

$$P(RNA = j) = \frac{\left(\frac{k_t}{\delta_{RNA}}\right)^j e^{-\frac{k_t}{\delta_{RNA}}}}{j!}, j = 0, 1, 2, 3, .. \tag{4}$$

The mean of the RNA is equal to the variance of the distribution, $\mu_{RNA} = Var_{RNA}$. Therefore, the Fano-factor and the noise (coefficient of variation, *CV*) are characteristic of the Poisson distribution:

$$\begin{aligned} Fano_{RNA} &= \frac{Var_{RNA}}{\mu_{RNA}} = 1 \\ \eta = CV_{RNA} &= \frac{\sqrt{Var_{RNA}}}{\mu_{RNA}} = \frac{1}{\sqrt{\mu_{RNA}}} \end{aligned} \tag{5}$$

Two-state promoter model

The RNA is transcribed only when the promoter is in the active state. The RNA is degraded by a first order process. The conservation equation, $I_i + A_i = 1$, indicates that the total number of the promoter is one.

$$I_i \xrightarrow{k_{ON}} A_i$$

$$A_i \xrightarrow{k_{OFF}} I_i$$

$$\emptyset \xrightarrow{A_i k_t} RNA_i$$

$$RNA_i \xrightarrow{\delta_{RNA}} \emptyset \tag{6}$$

The Fano-factor is greater than one for all positive values of the parameters in Equation 10, which implies a super-Poisson distribution.

Two-state promoter model with fluctuations in degradation

The enzyme that degrades the RNA is modeled explicitly. The enzyme is produced and degraded in a birth-death process, $k_{E,DEG} = \mu_{E,DEG} \cdot \delta_{E,DEG}$, where $\mu_{E,DEG} = \langle E_{DEG} \rangle$ denotes the mean steady-state concentration of the enzyme. Thus, intensity of fluctuations is tuned by varying$\mu_{E,DEG}$. The $E_{DEG}/\mu_{E,DEG}$ ratio represents the dimensionless fluctuations. $\tau_{1/2}(E_{DEG}) = Ln[2]/\delta_{E,DEG}$.

$$
\begin{aligned}
I_i &\xrightarrow{k_{ON}} A_i \\
A_i &\xrightarrow{k_{OFF}} I_i \\
\varnothing &\xrightarrow{A_i k_t} RNA_i \\
RNA_i &\xrightarrow{\frac{E_{DEG}}{\langle E_{DEG}\rangle}\delta_{RNA}} \varnothing \\
\varnothing &\xrightarrow{k_{E,DEG}} E_{DEG} \\
E_{DEG} &\xrightarrow{\delta_{E,DEG}} \varnothing
\end{aligned}
\tag{7}
$$

Two-state promoter model with fluctuations in RNA synthesis

The enzyme that synthesizes the RNA, the RNA polymerase, is modeled explicitly. The enzyme is produced and degraded in a birth-death process, $k_{E,SYN} = \mu_{E,SYN}\delta_{E,SYN}$, where $\mu_{E,SYN}$ denotes the mean steady-state concentration of the enzyme.

$$
\begin{aligned}
I_i &\xrightarrow{k_{ON}} A_i \\
A_i &\xrightarrow{k_{OFF}} I_i \\
\varnothing &\xrightarrow{A_i\frac{E_{SYN}}{\langle E_{SYN}\rangle}k_t} RNA_i \\
RNA_i &\xrightarrow{\delta_{RNA}} \varnothing \\
\varnothing &\xrightarrow{k_{E,SYN}} E_{SYN} \\
E_{SYN} &\xrightarrow{\delta_{E,SYN}} \varnothing
\end{aligned}
\tag{8}
$$

Two-state promoter model with fluctuations in RNA synthesis and degradation (Complete model)

The complete model combines the fluctuation in RNA synthesis and degradation in the models (7) and (8). We used this model to estimate the fluctuations in RNA synthesis and degradation based on the experimental data.

Parameter estimation to characterize the fluctuations in RNA synthesis and decay

The parameter estimation was performed in three stages (Table S5). First, analytical approaches were used, followed by stochastic simulations - a common approach in the parameter estimation of stochastic models (Aguilera et al., 2017).

In the first stage, we constrained the parameter values in the two-state promoter model with no external fluctuations (“Two-state promoter model,” (6)). The mean value of the RNA number μ_{RNA} is given by:

$$
\mu_{RNA} = \frac{k_{ON}}{k_{ON}+k_{OFF}}\frac{k_t}{\delta_{RNA}} \tag{9}
$$

An explicit analytical expression is known for the variance of the RNA distribution (Peccoud and Ycart, 1995), from which the Fano-factor can be obtained.

$$
Fano_{RNA} = \frac{Var_{RNA}}{\mu_{RNA}} = 1 + \frac{k_{OFF}}{k_{ON}+k_{OFF}}\frac{k_t}{k_{ON}+k_{OFF}+\delta_{RNA}} \tag{10}
$$

The Fano-factor is a useful measure of variability when the absolute molecule numbers are known (Paulsson, 2004; Thattai and van Oudenaarden, 2001). The mean and variance are determined by four parameters (the relevant rates are indicated in the parenthesis): k_t (RNA synthesis), δ_{RNA} (RNA decay), k_{ON} (promoter activation), k_{OFF} (promoter inactivation). The mRNA half-life (and thus δ_{RNA}) was fitted directly (Equation 2). Thereafter, three unknown parameters remain in the equations, k_{ON}, k_{OFF} and k_t. In order to determine the values of these three parameters, three equations with three measured variables have to be set up. Two of the variables were determined experimentally in this study, the $Fano_{RNA}$ and μ_{RNA}, since smFISH delivers absolute numbers. As the third variable, we have taken the fractional saturation of the promoter (*sat*), which has been measured for related GAL promoters by titration experiments (Gencoglu et al., 2017).

$$
sat = \frac{k_{ON}}{k_{ON}+k_{OFF}} \tag{11}
$$

sat = 0.62 for a GAL promoter with a single binding site. Promoters with multiple binding sites, such as the *GAL1* promoter, reach a higher saturation (Gencoglu et al., 2017). Thus, we have taken a realistic range: *sat* = 0.7 and 0.95. Solving the system of three equations, (9), (10) and (11), yields the three parameters in the two-state promoter model, as a function of saturation.

In the second stage, we extended the model with fluctuations in the RNA synthesis and degradation, and estimated the relevant fluctuation parameters by scanning. We simulated the steady-state and decay (see Complete model) for all parameter combinations in a 4-dimensional matrix $(n \cdot n \cdot m \cdot m)$. The $n \cdot n \cdot m \cdot m$ matrix was defined for each value of the promoter saturation (*sat*), with the following ranges unless stated otherwise. n = 1.25, 2.5, 5, 10, 20, 40, 80, 160 and 320 for $\langle E_{SYN} \rangle$and$\langle E_{DEG} \rangle$, which determine the intensity of the extrinsic fluctuations. m = 4, 8, 16, 32, 64 and 128 min for $Ln[2]/\delta_{E,SYN}$and $Ln[2]/\delta_{E,DEG}$, which determine the life-time (and hence the frequency) of the fluctuations.

We used the sum of squared error (SSE) to assess the goodness of the fit, calculated separately for each dataset (time series of extrinsic noise, histograms and mean decay profile). In this second stage, we calculated the SSE for two observations: (1) initial, steady-state distribution of mRNAs expressed from both alleles in a single replicate and (2) the extrinsic noise as a function of the mean as it changes over the decay time course, including the initial time point (t = 0), performed in two replicate experiments. The *SSE* was then normalized to the lowest *SSE* value for each observation, yielding the relative *SSE*, *RSSE*. Thus, the theoretical minimal value (possible best fit) for the combined *RSSE* is 2.

As the output of the second stage, the 20 best fits, based on the combined *RSSE*, were collected and their extremal values defined the constrained parameter range for the third stage.

In the third stage, we simulated 5000 random parameter values from the ranges as defined below. For the enzyme fluctuation parameters, we have taken the ranges defined at the end of stage two and extended it by a factor of $\sqrt{2}$ on each side of the range. We have taken the most representative saturation. Furthermore, we have permitted the half-life to vary by a factor of $\sqrt{2}$ on each side to allow for the deviation between the deterministic value and stochastic mean RNA numbers. To compensate this variation, the transcription rate was determined so that the mean steady-state value of the RNA is restricted to the range between $0.83\mu_{RNA}$ and $1.1\mu_{RNA}$.

At the end of the third stage, the RSSE was calculated for three datasets. In addition to the two RSSEs as defined in the second stage (extrinsic noise time series and steady-state histogram), we fitted the half-life to the decay time series, using the complete stochastic model. The best fit represents the parameter combination in this refined range with the lowest sum of RSSEs.

Analysis of the single cell data

For the estimation of the half-life and basal expression, we have used the mean RNA values over the entire time-series. In the second and third stages of the fitting, we have applied two criteria to exclude data points of insufficient quality. First, we calculated noise only for those time points when the mean value of each RNA reporter was at least 0.8 molecule / cell. In this way, the fitting is not affected by measurements errors due to the low RNA numbers, which becomes more frequent at the later points of the time series. Second, if the mean value of the two reporter genes differed by more than 1.42 times then we excluded those data points from the analysis.

The parameter estimation of the semi-shutoff system was performed similarly as with the dual-reporter system but the extrinsic noise was substituted by the Pearson correlation coefficient. We estimated the parameters by fitting to the three observations: the initial steady-state distribution, the correlation as a function of the mean during the decay and the mean mRNA value as a function time. The correlation here is reminiscent of autocorrelation since one of the gene reporters remains in the steady-state.

Stochastic simulation

For each simulation, 10,000 runs were performed using StochKit (Sanft et al., 2011). Before the simulation of the decay process, the steady-state expression was reached by a pre-run. The initial value of the RNA in the pre-run was equal to the deterministic steady-state values (Equation 2). The following durations were defined for the pre-runs: 60 min for *TSL1* (WT) and *PGK1-PMS*, 240 min for *PGK1* and 360 min for *TSL1* (Δ*xrn1*).

The RNA decay was initiated by lowering the value of $k_t$so that the new steady-state expression is defined by the basal expression, RNA_b (fitted in (2)).